J. Fluid Mech. (1970), *vol.* 44, *part* 4, *pp.* 767–779
Printed in Great Britain

Interaction of grid turbulence with a uniform mean shear

By W. G. ROSE

Department of Aerospace Engineering and Engineering Physics,
The University of Virginia

(Received 3 March 1970)

Experiments to explore the effect of initial disturbance length-scale on turbulence developed in the presence of a uniform mean shear are the subject of this paper.

Flows with nearly the same mean shear ($8{\cdot}6\,\mathrm{sec}^{-1}$) and initially different turbulent scales are generated in a wind tunnel test-section by placing grids just downstream of a honeycomb of uniform cell diameter ($\frac{1}{4}$ in.) and non-uniform cell length. Both round-rod grids of uniform square mesh and parallel-rod construction with roughly equal solidity (0.34) are used. Grid mesh sizes range from $\frac{1}{24}$ in. to 2 in.

From the results it is concluded that for a given value of mean shear the imposed length scale fixes the energy level of the resulting turbulence, provided the scale is sufficiently large. When it is reduced below some minimum value the turbulence decays. Also, it is found that two-dimensional flow-generator geometries are more effective than three-dimensional geometries in producing a roughly homogeneous turbulent field with a higher fluctuation level in a shorter distance.

1. Introduction

Knowledge as to the fate of a finite disturbance in a uniform shear flow and identification of the parameters that control the dynamical processes involved are the aims of the present experiments.

Theoretical work on this problem has been concerned, for the most part, with initially 'weak' turbulent fields and has neglected the inertia terms containing triple correlations. On this basis, Deissler (1961) and Fox (1964), who retain the viscous terms and postulate an initially isotropic spectrum, find that the lateral fluctuations decay and the streamwise component grows with increasing time.† Similar results are obtained by Moffatt (1965) for the development of an initially plane disturbance with arbitrary orientation, neglecting viscous effects.

Hasen (1967) treats the case of a finite disturbance and her analysis of the non-linear equations results in an expression for a 'stability barrier'. The value of this parameter is determined by the initial length-scale of the disturbance and the magnitude of the mean-shear. It dictates the decay or persistence of the disturbance.

At this point, it seems reasonable to suspect that weak turbulence corresponds to a state that, judged by Hasen's criterion, should decay. The fact that growth

† For a recent extension of this work see Deissler (1970).

of the streamwise fluctuation is predicted by the results of weak turbulence theory can be accounted for by the neglect of the triple correlations. This eliminates the mechanism for spectral transfer of energy to the higher wave-numbers and more efficient dissipation. As production is present and feeds energy directly to the streamwise fluctuations it is not surprising that energy accumulates in this component.

To date, experiments concerned with turbulence in a uniform mean-shear flow (Rose 1966; Champagne, Harris & Corrsin 1970) have not investigated the effect of initial conditions on the properties of the 'nearly' homogeneous fields realized in these experiments, which is the ultimate goal of the present work.

Thus far only one aspect of this problem has been attempted, viz. investigation of the effect of initial disturbance length-scale on the development of turbulence in a uniform mean-shear flow. In order to facilitate systematic investigation of a large range of scale magnitudes, detailed measurements have been avoided and emphasis placed on qualitative evaluation of the results.

2. Experimental facility

An open-return wind tunnel with a 22:1 contraction ratio and a 2 ft. × 2 ft. × 20 ft. test-section, with its walls adjusted to provide a uniform test-section pressure field, is the basic tool. At a mean-velocity of 50 ft./sec, which is the average mean velocity used throughout the tests, the free-stream turbulence plus linearized constant-temperature hot-wire† noise corresponds to an equivalent turbulence level of about 0·10 %. The air stream is filtered‡ at the tunnel inlet and the mean air-temperature is continuously monitored. Corrections for variations from the calibration temperature are made (Rose 1962). The heated wire sensing element is 0·00015 in. tungsten about $\frac{3}{4}$ mm in length.

A sealed sliding box arrangement is located at the upstream end of the test-section and approximately 5 ft. downstream from the discharge of the contraction. It has two compartments: one is empty and it is inserted into the tunnel circuit when hot-wires are calibrated, the other contains the shear-flow generator and it is inserted to establish the test conditions.

3. Shear-flow generator

A honeycomb with hexagonal cell cross-section and uniform cell diameter of $\frac{1}{4}$ in. and non-uniform cell length, figure 1, is used to generate a basic shear flow. This basic flow is modified by placing grids of different geometries 6 in. downstream of the honeycomb discharge.

Without a grid, the honeycomb generates a nearly uniform mean-shear of 12·2 sec^{-1} at an average mean-velocity of 50 ft./sec, figure 2. When uniform geometry square-mesh grids of roughly equal solidity ($\sigma = 0{\cdot}34$) are added, the flows developed downstream of these grids retain a nearly uniform mean shear of reduced magnitude 8·6 ± 5 %, figure 4.

† Disa type 55D01 anemometer and type 55D10 linearizer.

‡ Farr Co. HP-200 disposable filters.

In all, seven square-mesh round-rod grids with mesh-sizes, M, ranging from $\frac{1}{24}$ in. to 2 in. and one parallel round-rod grid with a 2 in. rod spacing are used (table 1). Except for the 1 in. square-mesh grid, which is a precision grid, the other grids are made of wooden dowel or stainless-steel screen set into plywood frames.

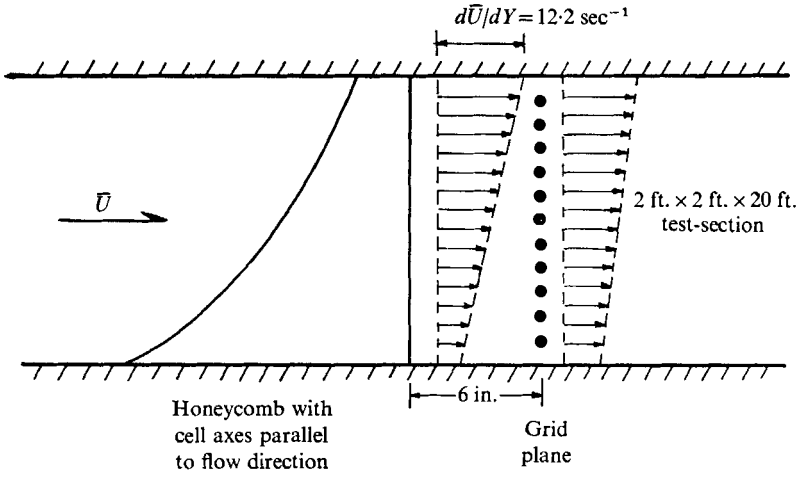

FIGURE 1. Flow generator.

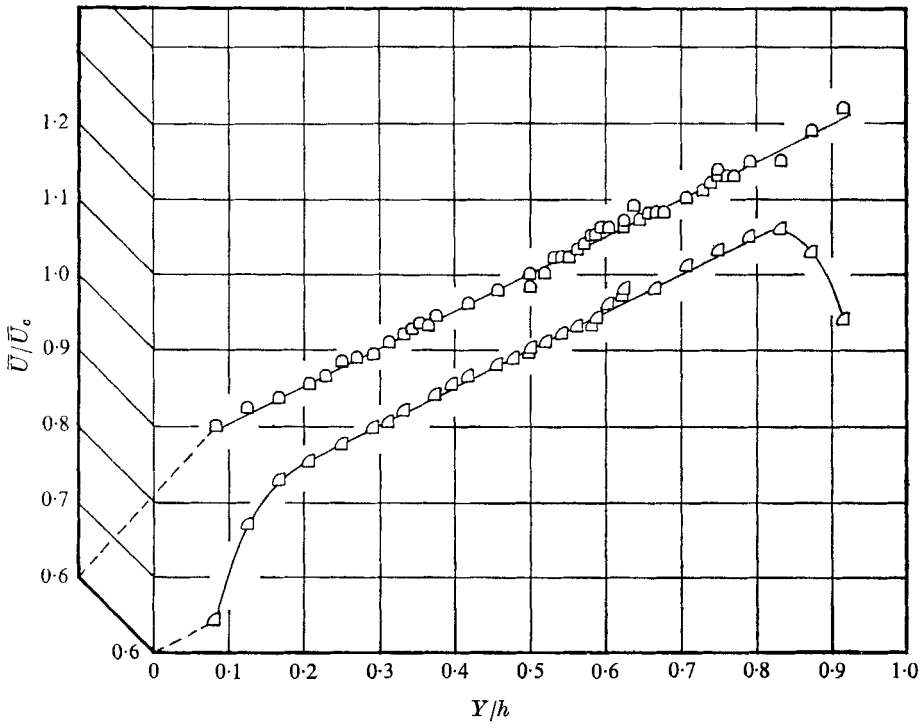

FIGURE 2. Honeycomb generated mean-shear distribution at: ⌓, $X/h = 1$; ⌓, $X/h = 8{\cdot}33$.

In order to eliminate laminar-to-turbulent transition of flow in the honeycomb cells, which introduces considerable unsteadiness in the test-section flow-fields at the test conditions, boundary-layer trips are placed on the leading edge of each cell wall. Trips are formed by looping 0·020 in. diameter wire to form a clip that is slipped over the cell leading-edge.

Grid		Solidity σ	Mean shear $d\bar{u}/dy(\text{sec}^{-1})$
Square mesh	$M = \frac{1}{24}$ in.	0·344	8·32
	$M = \frac{1}{12}$ in.	0·377	8·29
	$M = \frac{1}{6}$ in.	0·338	8·07
	$M = \frac{1}{3}$ in.	0·342	8·75
	$M = \frac{1}{2}$ in.	0·347	8·94
	$M = 1$ in.	0·348	8·75
	$M = 2$ in.	0·348	9·28
Honeycomb no grid		—	12·2
2 in. parallel rod		0·312	7·09 axes normal to gradient
2 in. parallel rod		0·312	6·07 axes parallel to gradient
Rose (1966)		—	13·6
Champagne, Harris & Corrsin (1970)		—	12·9

TABLE 1

4. Results

Honeycomb generated flow

The mean-velocity distribution generated by the honeycomb is shown in figure 2 where $\bar{U}$ is the only non-zero mean-velocity component and is associated with the X co-ordinate direction with origin located at the honeycomb discharge. All velocities are non-dimensionalized by the average mean velocity, $\bar{U}_c$, and all co-ordinate distances by the square test-section lateral dimension, h.

Two curves are given on figure 2 corresponding to $X/h = 1$, which is the upstream end of the test-section, and $X/h = 8{\cdot}33$, which is close to the downstream end. In each curve the straight-line drawn through the central, or core, region has the same slope. Aside from boundary-layer growth, the distinctive features of these distributions are the departures from a uniform mean shear in the regions corresponding to $Y/h = 0{\cdot}35$ and $0{\cdot}6$. These non-uniformities persist the length of the test-section.

Figure 3 gives the corresponding distributions of the r.m.s. value of the fluctuating streamwise velocity-component, $\tilde{u}$. It is evident that the mean-shear gradients in the regions near $Y/h = 0{\cdot}35$ and $0{\cdot}6$ are responsible for locally higher turbulence production. Although the average fluctuation level, as indicated by the faired curves, tends to a more uniform value downstream, these higher turbulent energy levels remain localized.

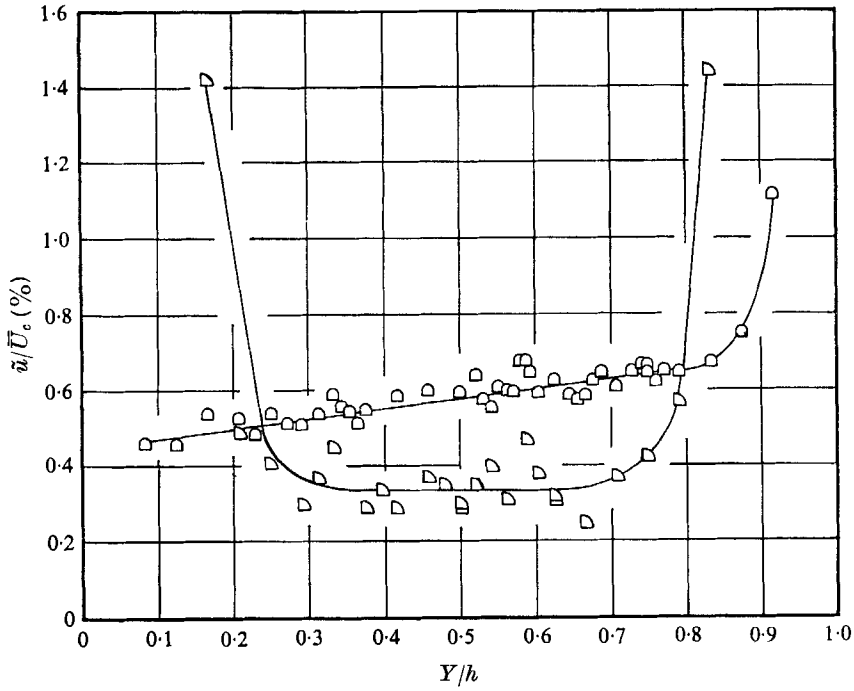

FIGURE 3. Honeycomb generated turbulence distributions at: ⌓, $X/h = 1$; ⌓, $X/h = 8{\cdot}33$.

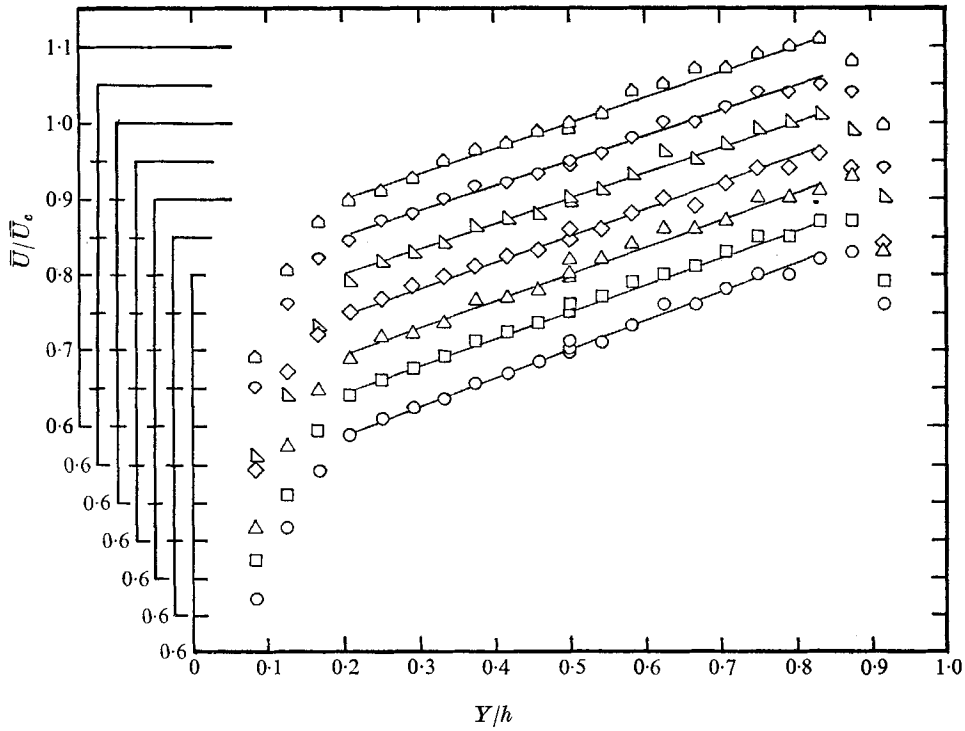

FIGURE 4. Square mesh grid mean-velocity profiles at $X/h = 1$. ⌓, $M = \frac{1}{24}$ in; ▽, $M = \frac{1}{12}$ in.; ◺, $M = \frac{1}{6}$ in.; ◇, $M = \frac{1}{3}$ in.; △, $M = \frac{1}{2}$ in.; □, $M = 1$ in.; ○, $M = 2$ in.

Honeycomb plus square-mesh grid generated flows

Similar results are presented in the next two figures for the square-mesh grids placed 6 in. downstream of the honeycomb discharge. Figure 4 gives the mean-velocity distributions at $X/h = 1$ where X is measured from the grid plane. The grid solidities and generated values of mean shear are given in the table. Distributions of the r.m.s. values of the fluctuations are shown in figure 5.

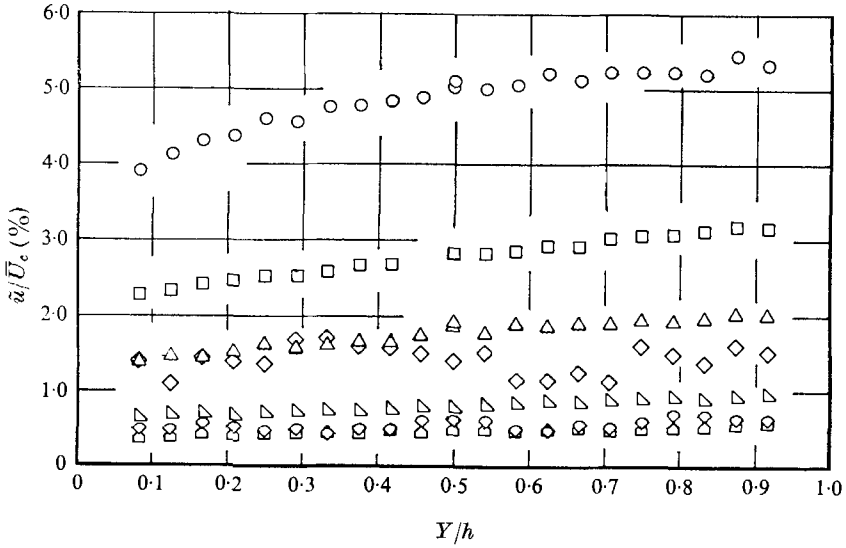

FIGURE 5. Square-mesh grid streamwise component of velocity fluctuation at $X/h = 1$. ⌓, $M = \frac{1}{24}$ in.; ▽, $M = \frac{1}{12}$ in.; ◺, $M = \frac{1}{6}$ in.; ◇, $M = \frac{1}{3}$ in.; △, $M = \frac{1}{2}$ in.; □, $M = 1$ in.; ○, $M = 2$ in.

Development of these flows along the length of the test-section is illustrated in figure 6. Its significant feature is the order of magnitude change in the downstream values of $\tilde{u}$. Less obvious, but important, the distances from the grids to the region where $\tilde{u}$ attains its 'asymptotic' values are roughly the same for all grids. Development of the free-stream fluctuation level plus instrument noise is shown on this figure, also.

Grid-flow conditions at the downstream end of the test-section are illustrated by figures 7 and 8 which give the mean-velocity and fluctuation distributions, respectively. For comparison, the straight lines faired through the mean-velocity distributions are the same as those used at $X/h = 1$.

Lack of $\tilde{u}$ uniformity, figure 8, leaves much to be desired when one is attempting to realize a homogeneous turbulent field. However, these non-uniformities are a result of localized departures from a uniform value of mean-shear in the basic mean-velocity profile, and non-uniformities in the grid geometries. In the case of the $\frac{1}{3}$ in. mesh grid, it has since been determined that dust accumulated while the grid is stored outside the tunnel contributes to its non-uniformity. The important result displayed in this figure is the near equality of the fluctuation levels attained by the $\frac{1}{6}$ in, $\frac{1}{12}$ in., $\frac{1}{24}$ in. grid flows with that of the free stream.

Honeycomb plus parallel-rod grid generated flows

Figures 9, 10 and 11 show the results of a cursory look at the fields generated by a parallel-rod grid placed the same distance downstream of the honeycomb discharge as were the square-mesh grids. As a simple check on the effect of rod

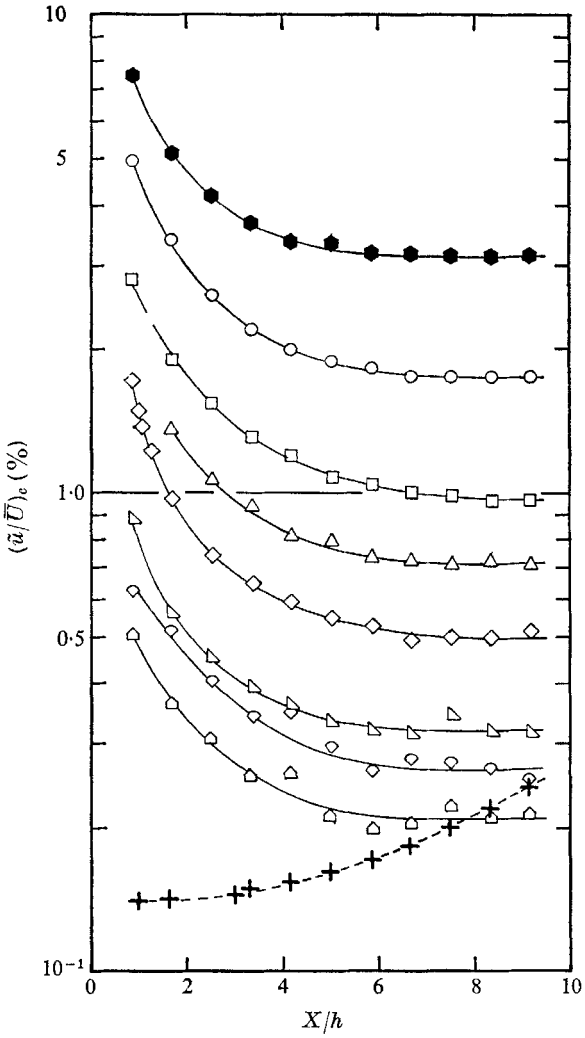

FIGURE 6. Turbulence development along the test-section centreline. ⌓, $M = \frac{1}{24}$ in.; ▽, $M = \frac{1}{12}$ in.; ◺, $M = \frac{1}{6}$ in.; ◇, $M = \frac{1}{3}$ in.; △, $M = \frac{1}{2}$ in.; □, $M = 1$ in.; ○, $M = 2$ in.; ⬢, no grid $\tilde{u}/\bar{U} \times 10$; +, free-stream plus instrument noise.

orientation with respect to the direction of the mean-velocity gradient, the grid was tested with its rods set both normal and parallel to the gradient. The grid rod centreline spacing is 2 in. and the rod diameter is $\frac{5}{8}$ of an inch. This gives a solidity about 10 % less than that of the square-mesh grids.

A comparison of the flow development downstream of the parallel-rod grids

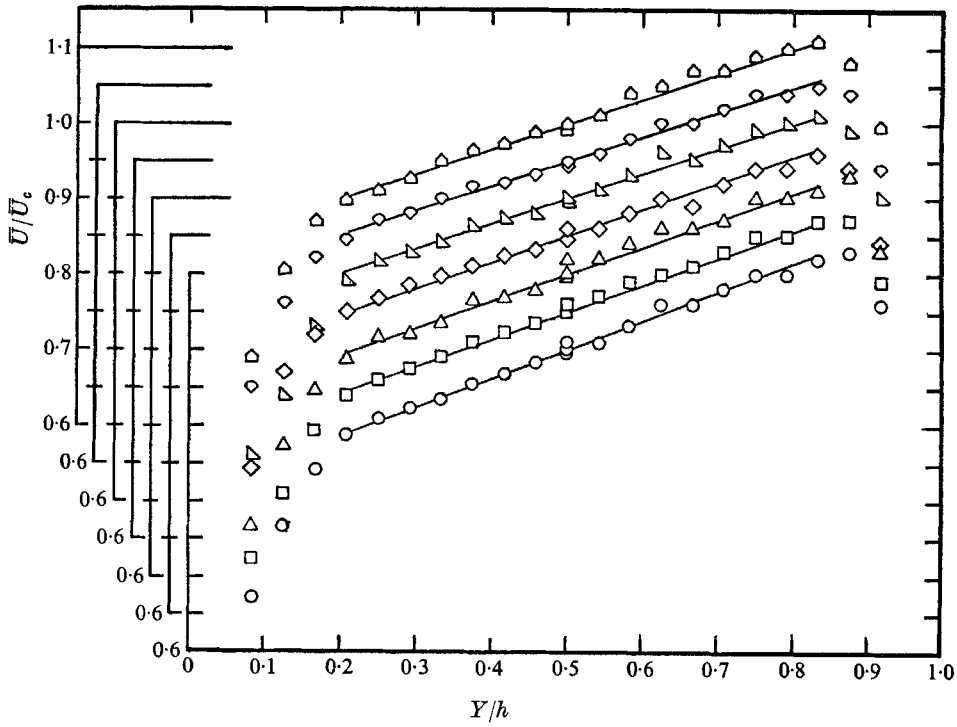

FIGURE 7. Square-mesh grid mean-velocity profiles at $X/h = 8{\cdot}33$. ⌓, $M = \frac{1}{24}$ in.; ▽, $M = \frac{1}{12}$ in.; ◺, $M = \frac{1}{6}$ in.; ◇, $M = \frac{1}{3}$ in.; △, $M = \frac{1}{2}$ in.; □, $M = 1$ in.; ○, $M = 2$ in.

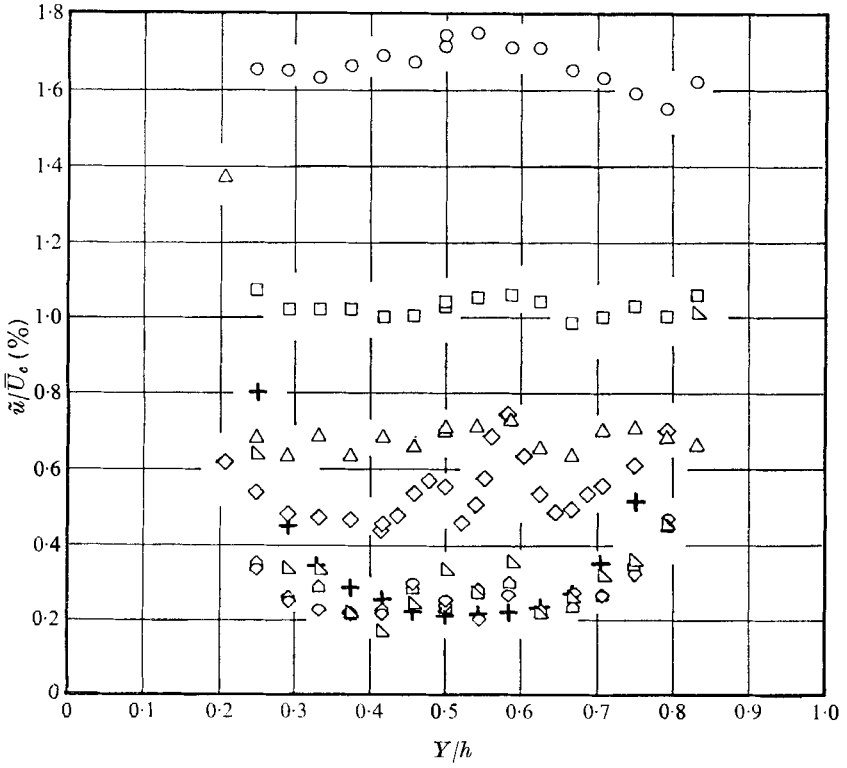

FIGURE 8. Square-mesh grid streamwise component of velocity fluctuation at $X/h = 8{\cdot}33$. ⌓, $M = \frac{1}{24}$ in.; ▽, $M = \frac{1}{12}$ in.; ◺, $M = \frac{1}{6}$ in.; ◇, $M = \frac{1}{3}$ in.; △, $M = \frac{1}{2}$ in.; □, $M = 1$ in.; ○, $M = 2$ in.; +, free-stream plus instrument noise.

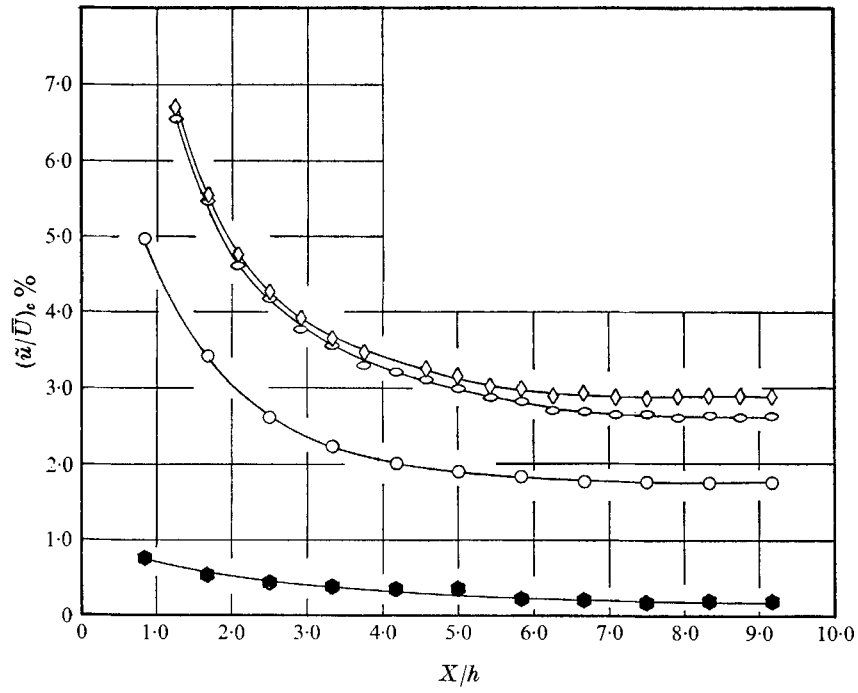

FIGURE 9. Centreline decay of parallel-rod grid turbulence. ◇, 2 in. parallel-rod axes norma to mean-velocity gradient; ○, 2 in. parallel-rod axes parallel to mean-velocity gradient; ○, 2 in. square-mesh grid; ⬢, honeycomb no grid.

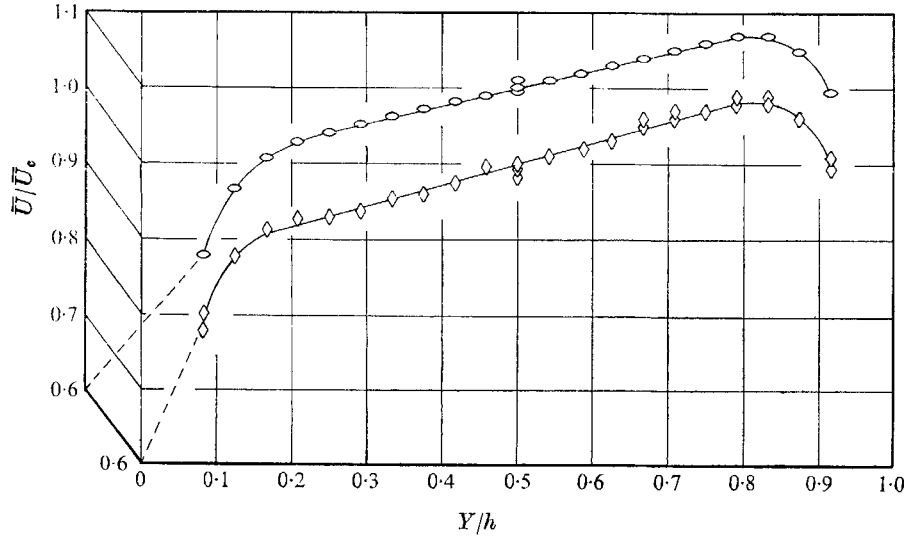

FIGURE 10. Parallel-rod grid mean-velocity profiles at $X/h = 8{\cdot}33$. ◇, 2 in. parallel-rod axes normal to mean-velocity gradient; ○, 2 in. parallel-rod axes parallel to mean-velocity gradient.

with that downstream of the 2 in. square-mesh grid is given in figure 9. The parallel-rod grids produce a higher resultant fluctuation level than does the square-mesh grid. In addition, although the development distances are closely the same for the parallel and square-mesh grid flows, the 10 % lower solidity of the parallel-rod grid, which one would expect to produce a higher mean shear, resulted in a mean shear of $7{\cdot}3\,\mathrm{sec}^{-1}$ when its rod axes are set normal to the gradient. This is 14 % lower than the mean shear generated by the higher solidity

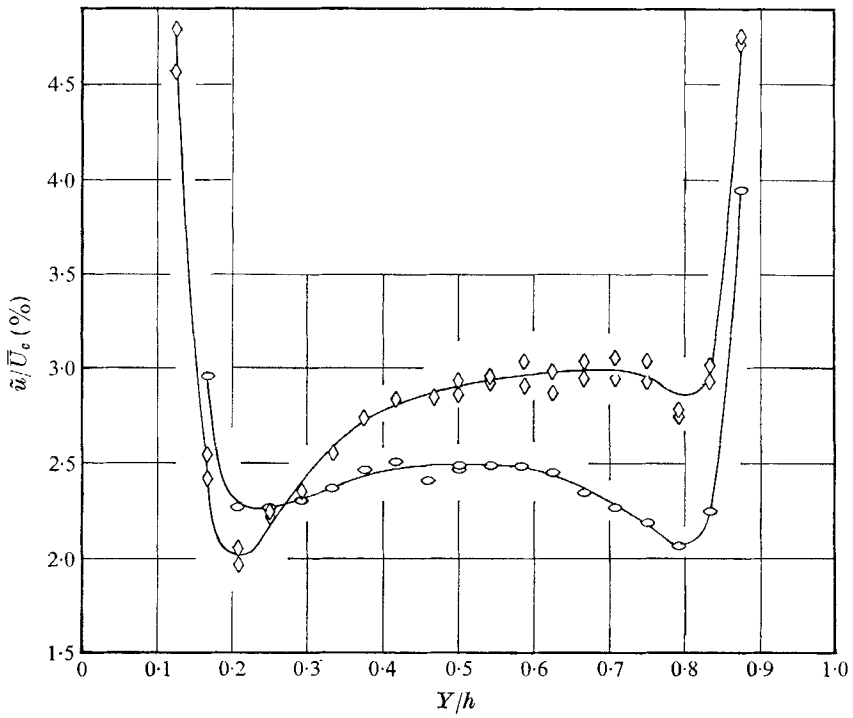

FIGURE 11. Parallel-rod grid turbulence at $X/h = 8{\cdot}33$. ◇, 2 in. parallel-rod axes normal to mean-velocity gradient; ○, 2 in. parallel-rod axes parallel to mean-velocity gradient.

2 in. square-mesh grid. There is an appreciable difference between the development distances corresponding to the parallel-rod grid with its axes normal and parallel to the gradient. The normal orientation gives a shorter distance and a slightly higher fluctuation level.

Mean-velocity distributions far downstream of the parallel-rod grids at $X/h = 8{\cdot}33$, and the corresponding distributions of the fluctuations levels, are shown in figures 10 and 11 respectively. An 18 % higher mean shear is obtained with the rod axes set normal to the gradient than with the axes set parallel to the gradient. Serious departures from uniform fluctuation levels are evident. They are best explained by the lack of uniform grid geometry.

5. Summary and discussion of results

An indication as to the validity of Hasen's stability barrier is best illustrated by figure 12 where the inverse mean-square fluctuation level is plotted as a function of the number of grid mesh-lengths downstream of the grid. Clearly,

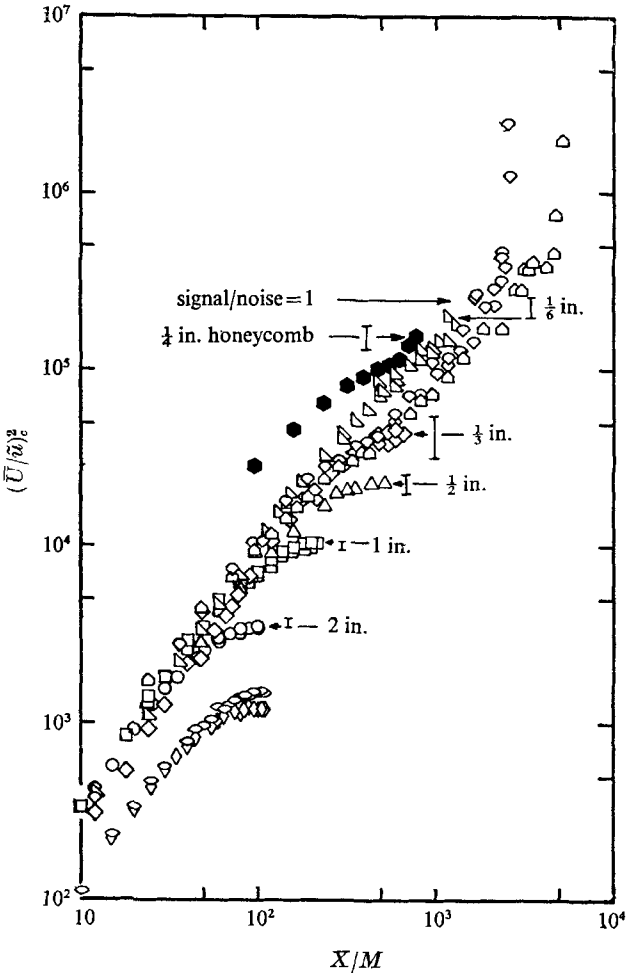

FIGURE 12. Turbulence development along the test-section centreline. ⌂, $M = \frac{1}{24}$ in.; ▽, $M = \frac{1}{12}$ in.; ◺, $M = \frac{1}{6}$ in.; ◇, $M = \frac{1}{3}$ in.; △, $M = \frac{1}{2}$ in.; □, $M = 1$ in.; ○, $M = 2$ in.; ⬢, honeycomb no grid; ◇, 2 in. parallel rod axes normal to mean-velocity gradient; ○, 2 in. parallel-rod axes parallel to mean-velocity gradient.

the turbulent fields generated by the $\frac{1}{24}$ in. and $\frac{1}{12}$ in. grids decay, while those generated by the $\frac{1}{3}$ in., $\frac{1}{2}$ in., 1 in., and 2 in. grids appear to level off at some asymptotic value. The final states attained by the $\frac{1}{4}$ in. honeycomb and the $\frac{1}{6}$ in. grid flows are not obvious. Error flags are shown to indicate the uncertainty in these values owing to the lateral non-uniformity of the downstream fluctuation levels. Uncertainty in the results for the $\frac{1}{24}$ in. and $\frac{1}{12}$ in. grids is not significant.

A convenient summary of the present results is obtained by introducing a characteristic velocity U^* defined in terms of the grid mesh-size, M, and the mean shear, $d\bar{U}/dy$, which gives $U^* \equiv M\,d\bar{U}/dy$. In figure 13 the ratios of the

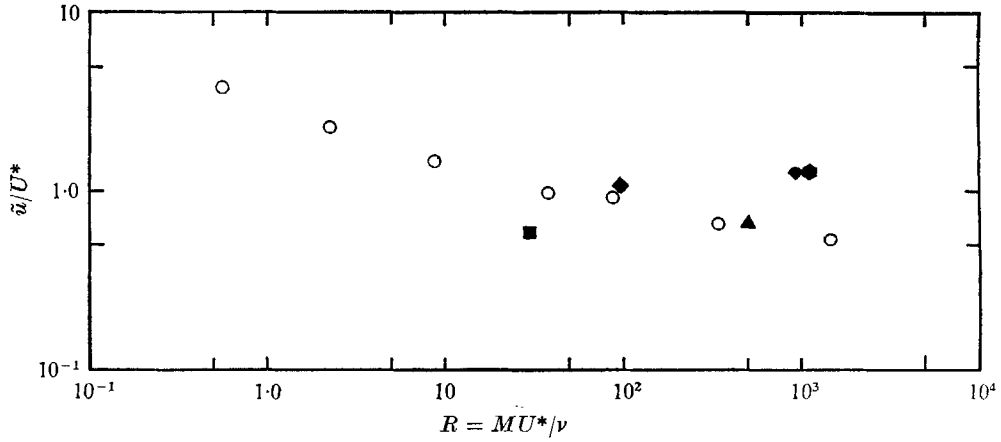

FIGURE 13. Comparison of measured streamwise component of velocity fluctuation, $\tilde{u}$, with the characteristic velocity $U^* \equiv M\,d\bar{U}/dy$. ○, square-mesh grids; ■, honeycomb no grid; ⬮, parallel-rod grid axes normal; ◆, parallel-rod grid axes parallel; ◆, Rose (1966); ▲, Champagne, Harris & Corrsin (1970).

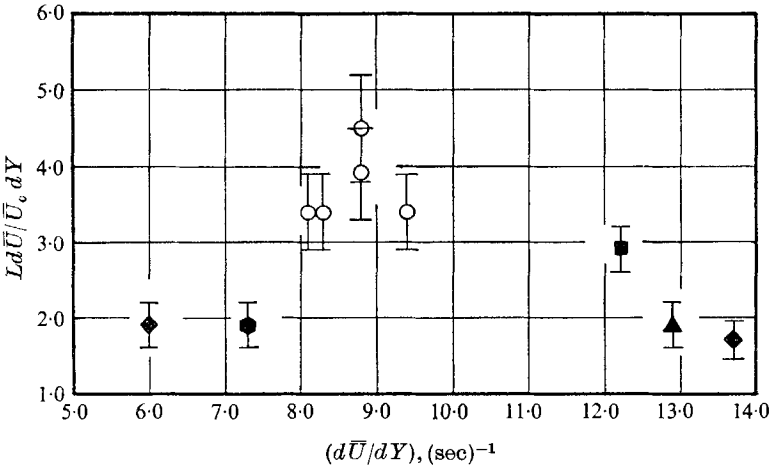

FIGURE 14. Comparison of measured flow development time, $L/\bar{U}_c$, with the characteristic time, $(d\bar{U}/dy)^{-1}$. ○, square-mesh grids; ■, honeycomb no grid; ⬮, parallel-rod axes normal; ◆, parallel-rod axes parallel; ◆, Rose (1966); ▲, Champagne, Harris & Corrsin (1970).

measured fluctuations, $\tilde{u}$, to U^* are shown for the range of $R = MU^*/\nu$ values generated in the present and previous experiments. Except for the smallest mesh grids, $U^* < 10^{-1}$ ft./sec where the turbulence decayed, the ratio is of order one. This corresponds to a value for the Reynolds number $R \equiv U^*M/\nu$ in the range of 1 to 10.

Although the effect of length scale is the principal point of the present work, the limited range of generated mean-shear magnitudes may be augmented by

those of previous experiments to assess the effect of mean-shear on the time for flow development. In figure 14 the quantity $(L/U_c)\,d\overline{U}/dy$ represents the ratio of two times. The length L is the measured distance from the flow generator to the region where the turbulence first attains its nearly uniform asymptotic state, e.g. where $\tilde{u}$ appears to assume a constant value. Consequently, the ratio $L/\overline{U}_c$, where $\overline{U}_c$ is the average mean-velocity, characterizes the measured flow-development time. The inverse mean shear is also a characteristic time. From figure 14, it is obvious that their ratio is of the order one.

It is interesting that the longer development times are associated with the square-mesh grids and the honeycomb, all of which have essentially three-dimensional geometries. The shorter times correspond to flow generators that have geometries that are more nearly two-dimensional.

6. Conclusions

For a given value of mean shear the length-scale of the initial disturbance fixes the energy level of the resulting turbulent field, provided the scale is sufficiently large. When it is reduced below some minimum value the turbulence decays. This minimum corresponds to a value of the Reynolds number $R = U^*M/\nu$ of order one.

It is found that two-dimensional flow-generator geometries are more effective than three-dimensional geometries in producing a roughly homogeneous turbulent field with a slightly higher fluctuation level in a somewhat shorter distance with the same mean-shear magnitude.

I wish to thank Mr Wen S. Hwang for his efforts in collecting and reducing data. This work was supported, in part, by the Air Force AFOSR under Grant AFOSR-1078-67. Construction of the wind tunnel facility and its instrumentation was aided by NSF Institutional Grant NSF GU-1022, and NASA Institutional Grant NSG-682.

REFERENCES

CHAMPAGNE, F. H., HARRIS, V. G. & CORRSIN, S. 1970 *J. Fluid Mech.* **41**, 81.

DEISSLER, R. G. 1961 *Phys. Fluids*, **4**, 1187.

DEISSLER, R. G. 1970 *Phys. Fluids*, **13**, 1868.

FOX, J. 1964 *Phys. Fluids*, **7**, 562.

HASEN, E. M. 1967 *J. Fluid Mech.* **29**, 721.

MOFFATT, H. K. 1965 *Stanford University Department of Aeronautics and Astronautics*, no. 242.

ROSE, W. G. 1962 *J. Appl. Mech.* **84**, 554.

ROSE, W. G. 1966 *J. Fluid Mech.* **25**, 97.